



Citation for published version:

Lin, J, Ngwompo, RF & Tilley, DG 2012, 'Development of a cardiopulmonary mathematical model incorporating a baro-chemoreceptor reflex control system', *Proceedings of the Institution of Mechanical Engineers, Part H - Journal of Engineering in Medicine*, vol. 226, no. 10, pp. 787-803. <https://doi.org/10.1177/0954411912451823>

DOI:

[10.1177/0954411912451823](https://doi.org/10.1177/0954411912451823)

Publication date:

2012

Document Version

Peer reviewed version

[Link to publication](#)

University of Bath

General rights

Copyright and moral rights for the publications made accessible in the public portal are retained by the authors and/or other copyright owners and it is a condition of accessing publications that users recognise and abide by the legal requirements associated with these rights.

Take down policy

If you believe that this document breaches copyright please contact us providing details, and we will remove access to the work immediately and investigate your claim.

Development of a cardiopulmonary mathematical model incorporating a baro-chemoreceptor reflex control system

J Lin¹, R F Ngwompo^{2*} and D G Tilley²

¹ Munich University of Applied Sciences', Dachauer Str. 98b, 80335 München

²Department of Mechanical Engineering, University of Bath, BA2 7AY, Bath, UK

Abstract

This paper describes the development of a comprehensive mathematical model of the human cardiopulmonary system that combines the respiratory and cardiovascular systems and their associated autonomous nervous control actions. The model is structured to allow the complex interactions between the two systems and the responses of the combined system to be predicted under different physiological conditions.

The cardiovascular system model contains 13 compartments including the heart chambers operating as a pump and the blood vessels represented as distensible tubes configured in a serial and parallel arrangement. The accurate representation of the hemodynamics in the system and the good fit to published pressure and flow waveforms gave confidence in the modelling approach adopted for the cardiovascular system prior to the incorporation of the baroreflex control and the respiratory models.

An improved baroreceptor reflex model is developed in this research incorporating afferent, central and efferent compartments. A sigmoid function is included in the efferent compartment to produce sympathetic and parasympathetic nerve outflow to the effector sites. The baroreflex action is modelled using physiological data, its interaction with the chemoreflex control is explained and the simulation results presented show the ability of the model to predict the static and dynamic hemodynamic responses to environmental disturbances.

A previously published respiratory model that includes the mechanics of breathing, gas exchange process and the regulation of the system is then combined with the cardiovascular model to form the cardiopulmonary model. Through comparison with published data, the cardiopulmonary model with the baro-chemoreflex control is validated

* Corresponding author: R.F.Ngwompo@bath.ac.uk

during hypoxia and hypercapnia. The percentage difference between the predicted and measured changes in the heart rates and the mean arterial pressures are within 3% in both cases. The total peripheral resistance correlates well for hypoxia but is less good for hypercapnia where the predicted change from normal condition is around 7% compared with a measured change of 23%. An example showing the application of the proposed model in sport science is also included.

Keywords: Cardiopulmonary systems; Baroreceptor reflex; Chemoreceptor reflex; Mathematical modelling.

NOTATION

A	Heart valve area (cm^2)
b	Bernoulli resistance term ($\text{mmHg}/(\text{ml/s})^2$)
e	Time varying elastance (mmHg/ml)
\hat{e}	Effective time varying elastance with septal coupling (mmHg/ml)
E	Elastance (mmHg/ml)
f	Frequency (Hz)
G	Gain
HR	Heart rate (beats/min)
k, K	Gain or Coefficient
k_{lr}	Left-to-right ventricular pressure gain
k_{rl}	Right-to-left ventricular pressure gain
L	Inertance ($\text{mmHg}/(\text{ml/s}^2)$)
MAP	Mean arterial pressure (mmHg)
P	Pressure (mmHg)
PNA	Parasympathetic neural firing rate (Hz)
Q	Flow (ml/s)
R	Resistance ($\text{mmHg}/(\text{ml/s})$)
s	Complex variable for Laplace transformation
SNA	Sympathetic neural firing rate (Hz)
t	Time variable (s)
t_{ac}	Time when atrium begins to contract (s)
t_{ar}	Time when atrium begins to relax (s)
t_{ee}	Time of end-ejection at maximum e_v (s)
T_r	Time period of cardiac cycle (s)
V	Volume (ml)
Φ	Volume constant (ml)
ρ	Density of blood (g/ml)

τ	Time constant (s)
τ_{ac}	Time constant for atrial contraction (s)
τ_{ar}	Time constant for atrial relaxation (s)
τ_{vc}	Time constant for ventricular contraction (s)
τ_{vr}	Time constant for ventricular relaxation (s)
Ω	Viscoelastance (mmHg · s/ml)

Subscripts

a	Atrium
aa	Aorta
aff	Afferent
b	Blood
c	Central compartment
it	Intrathoracic
l	Length for vascular segment
lv	Left ventricle
mv	Mitral valve
pc	Pericardium
r	Radius for vascular segment
R	Arterioles
s	Interventricular septum
\hat{s}	Sympathetic nerve activity
rv	Right ventricle
v	Ventricle
\hat{v}	Vagal (parasympathetic) nerve activity
V	Veins
v/v	Heart valves

1. INTRODUCTION

During the past five decades, the application of mathematical modelling to the cardiovascular and respiratory systems has received considerable interest with the aim that such an approach could assist in understanding the function and effects of the diseases associated with these two systems. With this purpose in mind, the models that have been developed to date tend to be limited to a particular function or disease. For example, some researchers have developed very complicated cardiovascular models without fully considering the effect of the respiratory

system [1-7] while others have concentrated on the development of the respiratory model but have ignored the important contribution of the cardiovascular system [8-11]. Since the 1980's, there has been a move to producing comprehensive cardiopulmonary models that allow the interaction between these two systems to be investigated [12-16]. This significantly broadens the application of the cardiopulmonary model.

The objective of the research reported here is to develop a comprehensive human cardiopulmonary model, including detailed representations of the respiratory and cardiovascular systems, which is capable of predicting the complex interactions between the two systems and their responses under different physiological conditions. A cardiovascular model including baroreflex is developed. This model is combined with a respiratory model that includes the gas exchange process and the antagonistic interaction of the baroreflex and the chemoreflex. The model is validated using published data and an example of the application of the model in the context of physical exercise is provided.

2. MODELLING THE CARDIOVASCULAR HYDRAULIC SYSTEM

In engineering terms, the cardiovascular system consists of a dual pump (heart), a series of distributing and collecting tubes (arteries and veins), and an extensive system of thin vessels that permit rapid gas exchange between the tissues and the vascular channels (capillaries). The heart consists of two pumps in series: one to pump blood through the lungs for exchange of oxygen (O_2) and carbon dioxide (CO_2) (the pulmonary circuit) and the other to circulate blood to all other tissues of the body (the systemic circuit). Unidirectional flow through the heart is achieved by the appropriate arrangement of effective flap valves.

The proposed model consists of 13 compartments including the pulmonary capillaries, the pulmonary arteries and veins, the left and right heart, the aorta, the systemic arteries and veins, the vena cava, the systemic capillaries, the intrathoracic compartment, the pericardium and the interventricular septum.

Nonlinearity aspects associated with the arteries are incorporated into the model to produce realistic arterial pressure and volume waveforms. However, the discontinuity of vein compliance due to venous collapse is not currently taken into account. The intrathoracic pressure is included as it is important to represent the interaction of the respiratory and cardiovascular systems. The characterisation of the individual compartments of the model are described in the following subsections.

2.1. Heart chambers

The heart is represented by a four-chamber model associated with the right and left ventricles and atria. Each chamber is modelled as a time-varying elastance model as proposed by Suga [17]. The elastance term e is assumed to vary over the cardiac cycle according to an exponential charge-discharge waveform and is characterised by a time constant τ , a baseline elastance E_b and an amplitude elastance term E_a [5].

The pressure-volume equations for the ventricles are given by

$$P_v = e_v V_v \quad (1)$$

$$\text{with } e_v = \begin{cases} E_{va} \left[1 - e^{-t/\tau_{vc}} \right] + E_{vb} & 0 \leq t \leq t_{ee} \\ (e_v|_{t_{ee}} - E_{vb}) e^{-(t-t_{ee})/\tau_{vr}} + E_{vb} & t_{ee} < t < T_r \end{cases} \quad (2)$$

where $e_v|_{t_{ee}}$ refers to the elastance at time t_{ee}

E_{va} and E_{vb} are the ventricle elastance amplitude and baseline values, respectively.

The equations for the atria are represented in a similar form

$$P_a = e_a V_a \quad (3)$$

$$e_a = \begin{cases} E_{aa} \left[1 - e^{-(t-t_{ac})/\tau_{ac}} \right] + E_{ab} & t_{ac} \leq t \leq t_{ar} \\ (e_a|_{t_{ar}} - E_{ab}) e^{-(t-t_{ar})/\tau_{ar}} + E_{ab} & t_{ar} < t < T_r + t_{ac} \end{cases} \quad (4)$$

where E_{aa} and E_{ab} are the atria elastance amplitude and baseline values, respectively.

The time period of the cardiac cycle is $T_r = 60 / HR$ where HR is the heart rate in beats per minute and the cardiac timing events specified by the values t_{ee} , t_{ac} and t_{ar} are described by linear approximations obtained by Beneken and De Wit [18]. These timing values are fed into the heart model to generate the cardiac activation functions.

2.2. Heart valves

The dynamics of the heart valves are described by Bernoulli's equation, which offers the possibility of investigating the acceleration/deceleration of the flow and the effect of valve stenosis [19]. This implies that the pressure drop caused by flow separation at the exit of the valve is proportional to the square of flow. An inertial term accounts for

the acceleration and deceleration of flow and viscous resistance is also included. The pressure-flow relation for a particular valve is given by

$$\frac{dQ_{vlv}}{dt} = \begin{cases} \frac{P_a - P_v - b_v Q_{vlv} |Q_{vlv}| - R_{vlv} Q_{vlv} + \Omega_a \dot{V}_a - \Omega_v \dot{V}_v}{L_{vlv}} & \text{for } P_a > P_v \\ 0 & \text{otherwise} \end{cases} \quad (5)$$

where $b_v = \rho / (2 \times 1333 A_{vlv}^2)$ with the constant term 1333 being a conversion factor when using pressure in mmHg.

2.3. Interaction between left and right heart

Interactions between the left and right heart include: (i) pressure coupling through the interventricular septum, (ii) volume coupling among the chambers in the pericardium, and (iii) hemodynamic coupling via the pulmonary circulation. The shift of the septum is represented by an elastic compartment using the approach described by Maughan *et al.* [20]. Under this assumption, the left ventricular pressure is the sum of the effective left ventricle elastance times the left ventricle volume and the “cross-talk” pressure from the right ventricle and is given by

$$P_{lv} = \hat{e}_{lv} V_{lv} + k_{rl} P_{rv} \quad (6)$$

where the right-to-left ventricular pressure $k_{rl} = e_{lv} / (E_s + e_{lv})$ and the effective elastance with septum coupling is

$$\hat{e}_{lv} = E_s k_{rl}.$$

Similarly, the right ventricle pressure is given by

$$P_{rv} = \hat{e}_{rv} V_{rv} + k_{lr} P_{lv} \quad (7)$$

$$\text{where } k_{lr} = e_{rv} / (E_s + e_{rv}) \text{ and } \hat{e}_{rv} = E_s k_{lr}$$

In addition to the pressure coupling between the ventricles, the volume coupling is included in all chambers in the pericardium. In the model proposed by Sun *et al.* [5], this is represented by a pericardial compartment with an exponential pressure-volume relationship given by

$$P_{pc} = K_{pc} e^{(V_{pc} - V_{pc0}) / \Phi_{pc}} \quad (8)$$

Φ_{pc} is the volume constant while V_{pc0} is the volume offset and K_{pc} is set to unity according to Sun’s model. V_{pc} is the sum of heart and pericardial fluid volumes and is set to be 30 ml under normal conditions.

2.4. Arteries, veins and capillaries

Arteries are represented by capacitance, resistance and inertance terms. Viscoelastance is also included though it has less effect on the flow dynamics than the other three terms. Nonlinearity is introduced to the capacitance using an exponential pressure-volume relationship. For the aorta, the pressure-volume relationship is given by [5]

$$\frac{dQ_{aa}}{dt} = \left[(P_{aa} - P_{sa}) - R_{aa} Q_{aa} + \Omega_{aa} \frac{dV_{aa}}{dt} - \Omega_{sa} \frac{dV_{sa}}{dt} \right] / L_{aa} \quad (9)$$

$$P_{aa} = E_{aa} \Phi_{aa} \quad (10)$$

$$E_{aa} = E_0 e^{V_{aa} / \Phi_{aa}} \quad (11)$$

Although the physiological characteristics of the veins are different from those of the arteries, Equations (9) - (11) can be used to describe the veins with some adjustment. A higher value is assigned to the volume constant Φ as the capacitance is relatively constant and veins are more compliant than arteries.

Nutrients and waste products exchange between blood and tissue in the capillaries, and for this reason, the capillaries must be included to form an overall circulatory model. The pulmonary capillaries share the same mathematical model as arteries and veins. This approach was used by Sun *et al.* [5] where good agreement with clinical data was obtained. From a physiological point of view, the systemic capillaries have a huge cross-sectional area which slows down the blood flow so that chemical metabolic energy exchange can take place. The resistance of the systemic capillaries is determined by the resistance of the arterioles supplying the systemic capillaries and by the number of open precapillary sphincters. As a result, the resistance is expected to play a dominant role, rather than capacitance and inertance in the systemic capillary model.

3. CARDIOPULMONARY MODEL INTEGRATION FOR SIMULATION AND CONTROL

A respiratory model, based on the model developed by Tomlinson *et al.* [11] was combined with the proposed cardiovascular model to form a detailed model of the cardiopulmonary system. The respiratory model of Tomlinson *et al.* [11] was used in the context of interaction with underwater breathing equipment and further improved through the incorporation of the mechanical and chemical control of breathing [21, 22].

The coupling between the respiratory and the cardiovascular systems includes the gas exchange process, the effect of breathing on the cardiovascular system and the blood gas contents on the hemodynamics. In the integrated cardiopulmonary model represented by the block diagram in Figure 1, the gas constituents (oxygen, carbon dioxide and nitrogen) pass through the nose and mouth to the tracheo-bronchial tree and reach the lung model where the gas exchange with the circulatory system takes place. The brain model detects the lung volume change and sends the required variation in thoracic force with respect to time to the pleural compartment. The pleural compartment model then calculates the pleural pressure acting on the lung to stimulate breathing. The gases quantified in terms of the constituents concentrations are carried by the blood from the lung to other cardiovascular compartments. The left and right heart models, which have pressure and volume coupling between the two chambers through the pericardium, pump the blood through the whole body.

4. DEVELOPMENT OF A CARDIOPULMONARY BARO-CHEMORECEPTOR CONTROL MODEL

For the regulation of the cardiopulmonary system, the schematic representation of the interaction between the chemoreflex and the baroreflex is shown in Figure 2. The peripheral chemoreceptor detects the change of the oxygen and carbon dioxide partial pressures (P_{O_2} and P_{CO_2}) in the brain artery and determines the operating point for the baroreceptor model. The central chemoreceptor is sensitive to the brain arterial P_{CO_2} and when it is stimulated, the gain of the sympathetic outflow is increased accordingly. The parasympathetic outflow and sympathetic outflow are sent to the effector sites which control the hemodynamic parameters including heart rate, cardiac contractility, venous unstressed volume and peripheral resistance.

The most important short-term regulation of the arterial pressure and cardiovascular function is performed by the baroreceptor reflex control system. The proposed model is represented as a three-compartment system: afferent, central and efferent compartments as shown in Figure 2. The input parameter to the arterial baroreceptor is the mean aortic pressure (MAP). The peripheral chemoreceptor detects the change of the oxygen and carbon dioxide partial pressures (P_{O_2} and P_{CO_2}) in the brain artery and sets the operating point for the baroreceptor model. The activity of sympathetic and parasympathetic nerves are passed to the effector sites including the heart, veins and arterioles. The central chemoreceptor is sensitive to the brain arterial carbon dioxide partial pressures and when it is stimulated the gain of the sympathetic outflow is increased accordingly. The four main parameters involved in the regulation are the heart rate, the cardiac contractility, the venous compliance and the peripheral resistance. These parameters are fed

into the hydraulic cardiovascular model and the resulting aortic pressure is fed back to the controller (the autonomous nervous system). The structure of the mathematical models for each compartment is described in the following sections using the Laplace transform for convenience as these will be represented later in block diagrams.

4.1. Afferent compartment

The mean arterial pressure (*MAP*) is used as the input to the afferent compartment. Carotid pressure is not used because this pressure is the same as the arterial pressure in the supine position. Since the mean aortic pressure is used as the input, the baroreceptor response to the change of pressure can be ignored. However, features such as pressure threshold and time delay are still included in the model.

The baroreceptor action potential frequency has a linear relationship with the mean arterial pressure within a pressure threshold [23]. At a particular steady pressure, there is a certain rate of discharge by the neurons in the baroreceptors. This rate increases when the arterial pressure rises and decreases when the pressure falls. A first order filter is used to represent the delay response to the pressure change and a gain element is used to represent the rate of discharge:

$$P_{aff} = G_{aff} \frac{MAP}{1 + \tau_{aff}s} \quad (12)$$

4.2. Central compartment

The primary integrating centre for the baroreceptor reflexes is a diffuse network of highly interconnected neurons called the medullary cardiovascular centre, located in the brainstem medulla oblongata. The central compartment compares the mean arterial pressure and the arterial pressure demand, and gives out the difference between the demanding and actual arterial pressures:

$$P_{error} = P_{aff} - \frac{P_{demand}}{1 + \tau_c s} \quad (13)$$

The demand pressure P_{demand} is the arterial pressure at the baroreflex operating point and again a first order filter is used to represent the delay through the central compartment.

4.3. Efferent compartment

The efferent compartment comprises parasympathetic (PNA) and sympathetic (SNA) divisions which exhibit a sigmoid shape between the pressure and the nerve activities [24]. The two sigmoid functions in the two divisions of the efferent nerve outflow are given by:

$$SNA = \frac{SNA_{max} + SNA_{min} e^{P_{error}/k_s}}{1 + e^{P_{error}/k_s}} (1 + \Delta G_{SNA}) \quad (14)$$

where

$$k_s = (SNA_{max} - SNA_{min}) / (4 * S_{\dot{s}}) \quad (15)$$

$$PNA = \frac{PNA_{min} + PNA_{max} e^{P_{error}/k_v}}{1 + e^{P_{error}/k_v}} \quad (16)$$

where

$$k_v = (PNA_{max} - PNA_{min}) / (4 * S_{\dot{v}}) \quad (17)$$

$S_{\dot{s}}$ and $S_{\dot{v}}$ are the slopes at the operating point of the sigmoid function.

4.4. Control of heart rate

Warner and Russell [25] investigated the effects of sympathetic and parasympathetic stimulation and the combined effect on the heart rate by stimulating these nerves to a particular frequency level. Three features were drawn from the experiments:

- (i) the heart rate rises faster than it falls back to the control level;
- (ii) the change in the heart rate due to sudden nerve stimulation is dependent on the frequency stimulated (this is more noticeable for sympathetic than parasympathetic nerve activity);
- (iii) the gain of the response is nonlinear.

Based on the above experimental observations, an overall block diagram for the control scheme for the heart rate is proposed in Figure 3. A variable time constant first order transfer function is included in the path of both nerve divisions at the effector sites to represent the different heart rate response to increment and decrement of the nerve frequency. An exponential relationship with the input nerve frequency is used for the sympathetic branch time constant. A second order polynomial function is used to represent the nonlinear steady state gain as proposed by Levy and Zieske [26]. However, the steady state gain is only valid when the stimulated frequency is less than 8 Hz.

According to experimental data obtained by Warner and Russell [25] and by Levy and Zieske [26], an exponential function limits the gain and time delays for both nerve divisions. Therefore, a pure time delay is included in both divisions.

The interactions between the two nerve divisions on the control of the heart rate are very complicated. Methods proposed by Warner and Russell [25] and Levy and Zieske [26], have been simplified, and combined to provide a more comprehensive form as follows:

$$HR = HR_0 + \Delta HR \quad (18)$$

$$\Delta HR = \Delta HR_{\hat{s}} + \Delta HR_{\hat{v}} + c \cdot \Delta HR_{\hat{s}} \cdot \Delta HR_{\hat{v}} \quad (19)$$

$$\Delta HR_{\hat{s}} = G_{\hat{s}} \frac{f_{\hat{s}} \cdot e^{-T_{\hat{s}} s}}{1 + \tau_{\hat{s}} s} \quad (20)$$

where

$$G_{\hat{s}} = G_{\hat{s}0}^k (1 - e^{-k_{\hat{s}} \cdot f_{\hat{s}}}) \quad (21)$$

$$k_{\hat{s}} = G_{\hat{s}0}^k / k_{\hat{s}0}^k \quad (22)$$

$$\tau_{\hat{s}} = \begin{cases} G_{\hat{s}0}^{\tau} \cdot e^{-k_{\hat{s}}^{\tau} \cdot f_{\hat{s}}} & \text{when } f_{\hat{s}} \text{ increases} \\ 25 & \text{when } f_{\hat{s}} \text{ decreases} \end{cases} \quad (23)$$

$$k_{\hat{s}}^{\tau} = G_{\hat{s}0}^{\tau} / k_{\hat{s}0}^{\tau} \quad (24)$$

$$\Delta HR_{\hat{v}} = G_{\hat{v}} \frac{f_{\hat{v}} \cdot e^{-T_{\hat{v}} s}}{1 + \tau_{\hat{v}} s} \quad (25)$$

where

$$G_{\hat{v}} = G_{\hat{v}0} (1 - e^{-k_{\hat{v}} \cdot f_{\hat{v}}}) \quad (26)$$

$$k_{\hat{v}} = G_{\hat{v}0} / k_{\hat{v}0} \quad (27)$$

$$\tau_{\hat{v}} = \begin{cases} 0.1 & \text{when } f_{\hat{v}} \text{ increases} \\ 0.8 & \text{when } f_{\hat{v}} \text{ decreases} \end{cases} \quad (28)$$

4.5. Other effector sites

Other effector sites including arterioles and veins share similar characteristics. Sympathetic nerve outflow sends a signal to the effector sites which include a static gain, a first order filter and a pure time delay as shown in equation (29). The first order filter and the pure time delay represent the main aspects of the response time pattern. It is worth noting that the gain for venous compliance is negative while the others are positive.

$$\sigma = G_{eff} \frac{SNA \cdot e^{-T_\sigma s}}{1 + \tau_\sigma s} \quad (29)$$

4.6. Chemical control of cardiovascular system

The relationship between the mean arterial pressures and the gas content in the blood is given by Rothe *et al* [27]:

$$\Delta MAP = \begin{cases} k_1 + k_2 \cdot P_{b,CO_2} + k_3 / P_{b,O_2} & P_{b,CO_2} > 40 \text{ mmHg and } P_{b,O_2} < 104 \text{ mmHg} \\ k_1 + k_2 \cdot 40 + k_3 / P_{b,O_2} & P_{b,CO_2} \leq 40 \text{ mmHg and } P_{b,O_2} < 104 \text{ mmHg} \\ k_1 + k_2 \cdot P_{b,CO_2} + k_3 / 104 & P_{b,CO_2} > 40 \text{ mmHg and } P_{b,O_2} \geq 104 \text{ mmHg} \end{cases} \quad (30)$$

where k_1 , k_2 and k_3 are set coefficients, and P_{b,O_2} and P_{b,CO_2} are the oxygen and carbon dioxide partial pressure in the blood, respectively.

The mean arterial pressure ΔMAP is the arterial pressure at the baroreflex operating point in the central compartment of the baroreflex model described above. Thus the resetting of the baroreflex is linked to the peripheral chemoreceptor.

The relationship between the percentage change of the sympathetic nerve activity gain and the P_{CO_2} is based on an experiment undertaken by Liroy and Trzebski [28] where the action of the baroreceptors, peripheral chemoreceptors, and lung-stretch receptors was excluded:

$$\Delta G_{SNA} = \begin{cases} k_4 \cdot P_{b,CO_2} + k_5 & P_{b,CO_2} > 40 \text{ mmHg} \\ k_4 \cdot 40 + k_5 & P_{b,CO_2} \leq 40 \text{ mmHg} \end{cases} \quad (31)$$

4.7. Regulation of cerebral blood flow

Local regulation of the cerebral circulation is predominant over other neural factors because, among the various body tissues, the brain is the least tolerant to ischemia (insufficient blood flow). Generally, the total cerebral blood flow is constant and shows excellent auto-regulation between about 60 and 160 mmHg mean arterial pressure [29]. The cerebral vessels are known to be sensitive to P_{CO_2} and brain O_2 supply. In addition, the flow is also influenced by metabolic factors and the following equations were used to calculate the responses of the cerebral blood flow adapted from Patterson *et al* [30]:

$$\dot{Q}_b = (Q_{b,metabolic} + \Delta Q_{b,O_2} + \Delta Q_{b,CO_2} - Q_b) / \tau_{Qb} \quad (32)$$

where

$$\Delta Q_{b,CO_2} = \begin{cases} 2.785 - 0.1323P_{b,O_2} + 2.6032 \times 10^{-3}(P_{b,O_2})^2 & P_{b,O_2} < 104 \text{ mmHg} \\ -2.324 \times 10^{-5}(P_{b,O_2})^3 + 7.6559 \times 10^{-8}(P_{b,O_2})^4 & \\ 0 & P_{b,O_2} \geq 104 \text{ mmHg} \end{cases} \quad (33)$$

$$\Delta Q_{b,CO_2} = \begin{cases} 2.323 \times 10^{-2} - 3.1073 \times 10^{-2}P_{b,CO_2} & P_{b,CO_2} < 38 \text{ mmHg} \\ + 8.0163 \times 10^{-4}(P_{b,CO_2})^2 & \\ -15.58 + 0.76P_{b,CO_2} - 1.295 \times 10^{-2}(P_{b,CO_2})^2 & P_{b,CO_2} > 44 \text{ mmHg} \\ + 9.39 \times 10^{-5}(P_{b,CO_2})^3 - 2.1745 \times 10^{-7}(P_{b,CO_2})^4 & \\ 0 & \text{otherwise} \end{cases} \quad (34)$$

5. SIMULATION RESULTS AND MODEL VALIDATION

In this section, the simulation of the complete cardiopulmonary system incorporating the reflex control, developed in the previous sections, is presented. The model validation is based on typical physiological data for healthy subjects published in the literature. First, the cardiovascular model developed in section 2 is validated and a sensitivity test is performed in order to identify the parameters that have a high impact on the predicted response. The proposed cardiovascular system is then combined with an existing respiratory model [11, 22] to form a cardiopulmonary system which is controlled by the proposed baro-chemoreceptor reflex model for validation of the complete system. The model was numerically implemented using the Bath/p dynamic simulation package developed at the University of Bath, which had been previously used to develop physiological models [21]. This software is based on a modular

modelling approach and uses a variable order and variable time-step numerical integration algorithm to solve the resulting algebraic and differential equations with respect to time.

5.1. Validation of the cardiovascular hydraulic model

Parameters were firstly estimated in terms of the physiological range or the order of magnitude for the parameter value. The vascular resistances and inertances were calculated on the basis of fluid dynamic laws and the dimensions of the anatomic compartments that the individual sections of the model represent [31]. The heart valve parameters (inertance, resistance, and Bernoulli term for each valve) were obtained from a study by Sun et al. [32] using Doppler echocardiography data. The values for the parameters that could not be found from literature were fine tuned within their physiological ranges by trial and error by inspection of the predicted pressure and flow waveforms. A major determinant of the circulatory dynamics is the vascular elastance, which is nonlinear and specified by two parameters (E_0 and Φ). For each elastance, these two parameters were iteratively adjusted until an acceptable representation for the hemodynamic waveforms and the average volume stored in the elastance was achieved. The volume constant Φ is generally of the same order of magnitude as the volume in the elastance. The baseline elastance for the contracting chambers were also determined on the basis of volume distribution in the heart.

Two criteria were used to justify the results: the representation of the baseline hemodynamics in various parts of the system and the fit to published pressure and flow waveforms.

To aid tuning the parameters, a sensitivity analysis was performed on the model based on a gain factor that defines the sensitivity of the model [5]

$$Sensitivity\ Gain = \frac{\% \text{ change of affected (hemodynamic) index}}{\% \text{ change of affected (model) parameter}} \quad (35)$$

The chosen hemodynamic indexes were data routinely measured to assess the physiological state of the cardiovascular system such as cardiac output, systolic/diastolic aortic pressures, end-diastolic right and left ventricular pressures, pulmonary arterial pressure, right and left ventricular volumes, mean right and left atria pressures, total pulmonary volume, total cardiac volume and systemic venous blood volumes [5].

The results of the sensitivity analysis showed that the simulated hemodynamics was insensitive to most individual model parameters such as inertance, capacitance, resistance and viscoelastance except for peripheral capillaries resistance. The systemic and pulmonary veins which account for the preload capacitances for the right heart and left

heart were sensitive and are a major determinant of cardiac output and aortic pressure. The pericardial volume offset was found to be the most sensitive parameter due to the constraint effect of the pericardium being dominant.

Figure 4 compares the predicted pressure waveforms obtained using the parameter values presented in Table A1 with the experimental traces obtained by Sugawara *et al.* [33]. Although Sugawara's results were derived from canine in-vivo data, pressure waveforms obtained for both human and dogs show similar responses. The main physiological characteristic difference between the hearts of dogs and humans is the diameter of the coronary sinus which is not included in the model [34].

The predicted heart valve flow rate shown in Figure 5 decreases to zero abruptly due to the closure mechanism which assumes that the valve flow ceases when the pressure gradient becomes zero. As the aortic valve closes and the aortic walls relax, a rebound pressure wave against the aortic valve occurs, known as the dicrotic notch. The shorter aortic valve opening period due to this closure mechanism results in a relatively less distinctive dicrotic notch in the aortic pressure as shown on the expanded time scale of the pressure waveform in Figure 4 at around 1.95 seconds. Backflow and noise during the pressure decreasing phase for the aortic and mitral valves are neglected since this level of detail is beyond the scope of the current work.

5.2. Validation of the cardiopulmonary baro-chemoreceptor control model

The validated cardiovascular system was then combined with an existing respiratory model [21] whose parameters given in Table A3 are obtained from Lo [22] for the respiratory model, from Rothe *et al* [27] for the peripheral chemoreceptor and from Liou and Trzebski [28] for the central chemoreceptor. The values of the parameters that define the baroreflex control mechanism are shown in Table A2. All the parameters have been assigned on the basis of clinical or physiological literature. Specifically, the time delay and the time constant for the first order filter are reported in [6] and the parameters regarding efferent compartment and heart rate control are based on the experimental data presented in [24].

The cardiopulmonary model was initially assessed without cerebral autonomic control to predict the response for a human at rest when quiet breathing in the supine position, with a heart rate of 70 beats per minute and a respiratory frequency of 12 breaths per minute. Simulations at these conditions gave results similar to typical values of partial O₂ and CO₂ pressures in various vessels of the circulatory system as published by Berne and Levy [24].

The proposed autonomic control model and the interactions between baroreceptors and chemoreceptors were assessed during hypoxia (gas mixture 12% O₂ and 88% N₂) and hypercapnia (gas mixture 5% CO₂ and 95% O₂).

First, the hypoxic gas mixture was used to stimulate the peripheral chemoreceptor. The changes in the alveolar partial pressure of CO₂ and O₂ following the step input of the inspired gas mixture introduced at 100 seconds are shown in Figure 6. As expected, during the denervation of the baroreceptor, the parasympathetic nerve outflow decreases and the sympathetic nerve outflow increases resulting in the increased heart rate, as shown in Figure 7, due to the predominance of the cardiac sympathetic over the cardiac vagal activation. However, when the baroreceptor and the chemoreceptor are both innervated, the activation of the chemoreceptors inhibits the baroreflex which leads to an increase in the blood pressure (Figure 8). The activation of the baroreflex caused by the increased blood pressure blunts the change of the sympathetic and parasympathetic outflows leading to smaller changes of the two autonomic division outflows and a smaller increase in the heart rate (Figure 9) compared to the case of a denervated baroreceptor. The total peripheral resistance only experiences very small changes as shown in Figure 10.

A quantitative comparison between the simulated results (steady-state percentage change in heart rate, mean arterial pressure and total peripheral resistance) obtained from the proposed model and the experimental results reported by Cooper *et al* [35] in humans' during hypoxia is shown in Figure 11. The agreement between the model and the experimental results is considered to be good (less than 1% difference) although the changes obtained from the model are slightly higher than those obtained from experiment. Therefore, the model is considered to be capable of simulating the resetting of the baroreflex by activating the chemoreceptor and the dynamic interaction of the baroreceptor and chemoreceptor reflexes.

In a similar manner, the effects of hypercapnia were simulated by applying an inspired gas mixture of 5% CO₂ and 95% O₂. To highlight the interaction between the central chemoreceptor and the other receptors of the autoregulatory model, Figures 12 and 13 present a quantitative comparison of simulation results and published experimental data with and without the activation of the central chemoreceptor. It is clear that without the central chemoreceptor, the model produces very different results to the experiment and the signs of the predicted changes are in the opposite direction to the measured data (Figure 12). However, when the central chemoreceptor is included, the model produces much more satisfactory results with the predicted heart rate and mean arterial pressure changes being within 3% of the measured values (Figure 13). For the total peripheral resistance, the predicted change from normal condition is around 7% compared with a measured change of 23% although it should be noted that the measurements

were subject to a $\pm 20\%$ variation. The results produced here justify the assumption that the central chemoreceptor has an effect on the gain of the sympathetic nerve activity.

6. CARDIOPULMONARY MODEL APPLICATIONS

The model developed in this paper for the cardiopulmonary system can be used for clinical, physiological or training applications. The modularity and the flexibility of the model are such that basic compartment and parameter models can be changed or adjusted to predict cardiac and respiratory responses under different physiological conditions such as healthy subjects during exercise or patients with lung or cardiac diseases. One example is given below for illustration in the context of sport science.

The cardiovascular and respiratory adjustments in exercise consist of a combination and integration of neural and local (chemical) factors [29]. The cardiopulmonary model developed here will be used to predict the cardiovascular and respiratory responses during exercise using typical measured traces from one experiment presented in Figure 14 obtained before and during exercise by Toska and Eriksen [36].

The baroreflex is generally considered not to be an important controller of the circulation during exercise because chronic denervation of the baroreceptors does not cause an obvious deficit in blood pressure stability or level once the responses to moderate-to-heavy exercise have stabilized [37]. However, referring to Figure 14, a sudden transient drop in blood pressure is apparent at the onset of exercise after baroreceptor denervation indicating that the baroreceptor reflex remained sensitive at the onset of exercise. This result is supported by Melcher *et al.* [38] who also presented clear evidence of maintained baroreflex sensitivity during exercise.

The effect of the baroreflex on the cardiovascular system at the onset of exercise can be simulated by shifting the operating point of the central compartment and locally inducing vasodilatation in the exercising muscles. Toska and Eriksen [36] recorded the responses of 10 healthy men at the onset of moderate, dynamic exercise while supine. The data used here for parameterisation is the average of the 10 responses. The shift of the operating point was estimated to be 7% by Elstad *et al* [39]. It should be noted that this shift is directly proportional to the intensity of exercise [40]. The vasodilatation can be modelled by decreasing the peripheral resistance with a time constant of 5.5 seconds [39]. An appropriate value for the resistance is estimated to be 0.18 mmHg· s/ml according to Toska and Eriksen's experiment [36].

The predicted cardiovascular responses at the onset of exercise at time 50s (indicated by the vertical dotted line) included in Figure 15 show the same trend as the experimental results shown in Figure 14. For example, after the onset of exercise, both the experimental and simulated heart rates increase by about 10 beats per minute. A transient decrease in stroke volume (indicated by the arrow on Figure 15) at the onset of exercise delays the increase in simulated cardiac output by a few seconds. The stroke volume then returns close to its resting level and the cardiac output increases in parallel with heart rate. Mean arterial pressure shows a transient decrease during the first few seconds of exercise before increasing to a level slightly above the resting value. The total peripheral conductance (reciprocal of total peripheral resistance) also increases to a higher level and then remains reasonably constant for the rest of the exercise period.

7. CONCLUSIONS

This paper describes the development of a comprehensive mathematical model of the human cardiopulmonary system that combines the respiratory and cardiovascular aspects and their associated control actions. The cardiovascular system model contains 13 compartments, including the heart chambers and the blood vessels, to represent the important features of the blood circulation. The parameters of the model are obtained from published clinical and physiological data and a sensitivity analysis is undertaken to provide guidance on the tuning of the model to achieve realistic blood pressure and flow waveforms to show good correlation with published experimental results. The validated cardiovascular model is then combined with an existing respiratory model, where the interactions between both systems are represented and a baro-chemoreceptor reflex control system is developed. The simulations of the complete control cardiopulmonary system show that the proposed model is capable of predicting the complex interactions between the cardiovascular system and the respiratory system. This has also been validated during hypoxia and hypercapnia through comparison with published data. The control algorithm explains the regulation of the cardiopulmonary system and allows further neuro-hormonal regulation mechanism to be easily integrated in the future.

The proposed model can be a useful tool in clinical demonstration and education as well as supporting research in areas including sport sciences. The response of the cardiopulmonary system during physical exercise is an example included in this paper for illustration. A future application envisaged for this research is an extension of the work of

Tomlinson et al [11] on the computer simulation of the human interaction with underwater breathing equipment with a more integrated and complete cardiopulmonary model.

REFERENCES

- 1 **Boyers, D. G., Luetsche, J. A., and Cuthbert, J. G.** Simulation of Human Cardiovascular System - Model with Normal Responses to Change of Posture, Blood Loss, Transfusion, and Autonomic Blockade. *Simulation*, 1972, **18**(6), 197-206.
- 2 **Hyndman, B. W.** A digital simulation of the human cardiovascular system. *Infor. J.*, 1972, **10**, 8-35.
- 3 **Leaning, M. S., Pullen, H. E., Carson, E. R., and Finkelstein, L.** Modelling a complex biological system: the human cardiovascular system. 2. Model validation reduction and development. *Transactions on Instrumentation, Measurement and Control*, 1983, **5**, 87-98.
- 4 **Sud, V. K., Srivasan, R. S., Charles, J. B., and Bungo, M. W.** Mathematical modelling of the human cardiovascular system in the presence of stenosis. *Phys. Med. Biol.*, 1993, **38**(3), 369-378.
- 5 **Sun, Y., Beshara, M., Lucariello, R. J., and Chiaramida, S. A.** A comprehensive model for right-left heart interaction under the influence of pericardium and baroreflex. *Am. J. Physiol*, 1997, 272(3 Pt 2), H1499-H1515.
- 6 **Ursino, M. and Magosso, E.** Role of short-term cardiovascular regulation in heart period variability: a modeling study. *American Journal of Physiology-Heart and Circulatory Physiology*, 2003, **284**(4), H1479-H1493
- 7 **Kim, H. J., Jansen, K. E. and Taylor, C. A.** Incorporating autoregulatory mechanisms of the cardiovascular system in three-dimensional finite element models of arterial blood flow. *Annals of Biomedical Engineering*, 2010, **38** (7), 2314–2330
- 8 **Zacek, M. and Krause, E.** Numerical simulation of the blood flow in the human cardiovascular system. *J Biomech.*, 1996, **29**(1), 13-20
- 9 **Grodins, F. S., Buell, J., and Bart, A. J.** Mathematical analysis and digital simulation of the respiratory control system. *J. Appl. Physiol.*, 1967, **22**(2), 260-276.
- 10 **Liu, C. H., Niranjana, S. C., Clark, J. W., Jr., San, K. Y., Zwischenberger, J. B., and Bidani, A.** Airway mechanics, gas exchange, and blood flow in a nonlinear model of the normal human lung. *J. Appl. Physiol.*, 1998, **84**(4), 1447-1469.
- 11 **Tomlinson, S. P., Lo, J. K. W., and Tilley, D. G.** Computer simulation of human interaction with underwater breathing equipment. *Proceedings of the Institution of Mechanical Engineers, Part H: Journal of Engineering in Medicine*, 1994, **208**(4), 249-261.
- 12 **Ben-Tal, A.** Simplified models for gas exchange in the human lungs. *Journal of Theoretical Biology*, 2006, **238**(2), 474-495.

- 13 Lu, K., Clark, J. W., Jr., Ghorbel, F. H., Ware, D. L., and Bidani, A. A human cardiopulmonary system model applied to the analysis of the Valsalva maneuver. *Am. J. Physiol Heart Circ. Physiol* , 2001, **281**(6), H2661-H2679.
- 14 Ursino, M., Magosso, E., and Avanzolini, G. An integrated model of the human ventilatory control system: the response to hypercapnia. *Clinical Physiology* , 2001, **21**(4), 447-464.
- 15 Ursino, M., Magosso, E., and Avanzolini, G. An integrated model of the human ventilatory control system: the response to hypoxia. *Clinical Physiology*, 2001, **21**(4), 465-477.
- 16 Lin, J. Mathematical modelling of the human cardiopulmonary system, PhD Thesis University of Bath, 2007.
- 17 Suga, H. Theoretical Analysis of A Left-Ventricular Pumping Model Based on Systolic Time-Varying Pressure/Volume Ratio. *IEEE Transactions on Biomedical Engineering*, 1971, **BM18**(1), 47-54.
- 18 Beneken, J. and Dewit, B. A physical approach to hemodynamic aspects of the human cardiovascular system. In *Physical Bases of Circulatory Transpport: Regulation and Exchange* (Eds E. Reeve & A. Guyton), 1967, 1-45.
- 19 Fung, Y. C. *Biodynamics: Circulation*. Springer-Verlag, New York, 1984.
- 20 Maughan, W. L., Sunagawa, K., and Sagawa, K. Ventricular systolic interdependence: volume elastance model in isolated canine hearts. *AJP - Legacy* , 1987, **253**(6 Pt 2), H1381-H1390.
- 21 Tomlinson, S. P., Tilley, D. G., and Burrows, C. R. Computer-Simulation of the Human Breathing Process. *IEEE Engineering in Medicine and Biology Magazine*, 1994, **13**(1), 115-124.
- 22 Lo, J. K. W., Mathematical modelling of mixed gas breathing equipment and associated systems. *PhD, University of Bath*, 1995
- 23 Itani, T. F. and Koushanpour, E. A mathematical model of the arterial baroreceptors. *Proceedings of the Annual International Conference of the IEEE Engineering in Medicine and Biology Society*, 1989, 289-299.
- 24 Kollai, M. and Koizumi, K. Cardiac Vagal and Sympathetic-Nerve Responses to Baroreceptor Stimulation in the Dog. *Pflugers Archiv-European Journal of Physiology*, 1989, **413**(4), 365-371.
- 25 Warner, H. R. and Russell, R. I. C. H. Effect of Combined Sympathetic and Vagal Stimulation on Heart Rate in the Dog. *Circulation Research*, 1969, **24**(4), 567-573.
- 26 Levy, M. N. and Zieske, H. Autonomic control of cardiac pacemaker activity and atrioventricular transmission. *Journal of Applied Physiology*, 1969, **27**(4), 465-470.
- 27 Rothe, C. F., Maass-Moreno, R., and Flanagan, A. D. Effects of hypercapnia and hypoxia on the cardiovascular system: vascular capacitance and aortic chemoreceptors. *Am. J. Physiol*, 1990, **259**(3 Pt 2), H932-H939.
- 28 Lioy, F. and Trzebski, A. Pressure effect of CO₂ in the rat: different thresholds of the central cardiovascular and respiratory responses to CO₂. *J. Auton. Nerv. Syst.*, 1984, **10**(1), 43-54.

- 29 **Berne, R. M. and Levy, M. N.** *Physiology*. 1988 (The C.V.Mosby Company, USA).
- 30 **Patterson, J. L., Jr., Goetz, R. H., Doyle, J. T., Warren, J. V., Gauer, O. H., Detweiler, D. K., Said, S. I., Hoernicke, H., McGregor, M., Keen, E. N., Smith, M. H., Jr., Hardie, E. L., Reynolds, M., Flatt, W. P., and Waldo, D. R.** Cardiorespiratory dynamics in the ox and giraffe, with comparative observations on man and other mammals. *Ann. N. Y. Acad. Sci.*, 1965, **127**(1), 393-413.
- 31 **Sun, Y.** Modeling the dynamic interaction between left ventricle and intra-aortic balloon pump. *AJP – Legacy*, 1991, **261**(4 Pt 2), H1300-H1311.
- 32 **Sun, Y., Sjoberg, B. J., Ask, P., Loyd, D., and Wranne, B.** Mathematical model that characterises transmitral and pulmonary venous flow velocity patterns. *AJP – Legacy*, 1995, **268**(1 Pt 2), H476-H489.
- 33 **Sugawara, M., Kajiya, R. D., Kitabatake, A., and Matasuo, H.** *Blood Flow in the heart and Large Vessels*. 1989 (Springer-Verlag, Tokyo).
- 34 **Iiazzo, P. A.,** *Handbook of Cardiac Anatomy, Physiology, and Devices*. 2005 (Humana Press, Totowa, New-Jersey).
- 35 **Cooper, V. L., Pearson, S. B., Bowker, C. M., Elliott, M. W., and Hainsworth, R.** Interaction of chemoreceptor and baroreceptor reflexes by hypoxia and hypercapnia - a mechanism for promoting hypertension in obstructive sleep apnoea. *The Journal of Physiology*, 2005, **568**(2), 677-687.
- 36 **Toska, K. and Eriksen, M.** Peripheral Vasoconstriction Shortly After Onset of Moderate Exercise in Humans. *Journal of Applied Physiology*, 1994, **77**(3), 1519-1525.
- 37 **Rowell, L. B., O’Leary, and D. S.** **Reflex** Control of the Circulation During Exercise - Chemoreflexes and Mechanoreflexes. *Journal of Applied Physiology*, 1990, **69**(2), 407-418.
- 38 **Melcher, A. and Donald, D. E.** Maintained ability of carotid baroreflex to regulate arterial pressure during exercise. *AJP - Heart and Circulatory Physiology*, 1981, **241**(6), H838-H849.
- 39 **Elstad, M., Toska, K., and Walloe, L.** Model simulations of cardiovascular changes at the onset of moderate exercise in humans. *Journal of Physiology-London*, 2002, **543**(2), 719-728.
- 40 **Walgenbach, S. C. and Donald, D. E.** Inhibition by Carotid Baroreflex of Exercise-Induced Increases in Arterial-Pressure. *Circulation Research*, 1983, **52**(3), 253-262.

APPENDIX A – Cardiopulmonary system parameters

Table A1 – Cardiovascular parameters

	Pulmonary arteries	Pulmonary capillaries	Pulmonary veins	Aorta	Systemic arteries	Systemic capillaries	Systemic veins	Vena cava
R (mmHg · s/ml)	0.01	0.04	0.005	0.04	0.8	0.2	0.005	0.005
L (mmHg · s ² /ml)	0.0005	0.0002	0.0005	0.0005	0.0005	0.0005	0.0005	0.0005
Q (mmHg · s/ml)	0.01	0.01	0.01	0.01	0.01	0.01	0.01	0.01
E_0 (mmHg/ ml)	0.001	0.08	0.01	1.5	0.04	0.005	0.001	0.05
Φ (ml)	20	100	270	20	550	100	3200	20

	Left ventricle	right ventricle	left atria	right atria			Pericardium
Q (mmHg · s/ml)	0.0001	0.0001	0.0005	0.0005		K_{pc} (mmHg)	1
E_b (mmHg/ ml)	0.07	0.05	0.09	0.06		V_{pc0} (ml)	380
E_a (mmHg/ ml)	6	0.7	0.07	0.04		Φ (ml)	40
						V_{pe} (ml)	30

	Mitral valve	Aortic valve	Tricuspid valve	Pulmonary valve			Intrathoracic pressure
R (mmHg · s ² /ml)	0.001	0.001	0.001	0.01		Pitb (mmHg)	-3.7
L (mmHg · s ² /ml)	0.0002	0.0005	0.0002	0.0005		Pita (mmHg)	-1.8
A (cm ²)	5	4	5	4		Tit (s)	0.1

t_r (s)	t_{ee} (s)	t_{ar} (s)	t_{ac} (s)	τ_{vc} (s)	τ_{vr} (s)	τ_a (s)
0.855	0.3	0.9	0.695	0.4	0.02	0.05

Table A2 – Baroreflex control parameters

Afferent compartment			$\tau_{aff} = 0.001 \text{ s}$ $G_{aff} = 1$
Central Compartment			$P_{demand} = 90 \text{ mmHg}$
Efferent compartment	Parasympathetic division		$S_p = 0.0205$ $PNA_{max} = 6 \text{ Hz}$ $PNA_{min} = 0.6 \text{ Hz}$
	Sympathetic division		$S_s = -0.0138$ $SNA_{max} = 4 \text{ Hz}$ $SNA_{min} = 1.12 \text{ Hz}$
Effector sites	Heart rate	Sympathetic division	$G_{s0}^k = 90 \text{ beats/min /Hz}$ $G_{s0}^r = 10 \text{ beats/min /Hz}$ $k_{s0}^k = 0.28$ $k_{s0}^r = 0.2$ $T_s = 3 \text{ s}$
		Parasympathetic division	$G_{v0} = 60 \text{ beats/min /Hz}$ $k_{v0} = 0.4$ $\tau_v = 0.1 \text{ s} / 0.8 \text{ s}$ $T_v = 0.5 \text{ s}$
		interaction between two divisions	$c = 0.017$ $HR_0 = 109 \text{ beats/min}$
	Myocardial constriction	left heart	$\tau_{\sigma,lv} = 1.5 \text{ s}$ $T_{e,lv} = 2 \text{ s}$ $G_{eff,lv} = 0.45 \text{ mmHg/ml/Hz}$ $E_{lv0} = 3 \text{ mmHg/ml}$
		right heart	$E_{rv0} = 0.1 \text{ mmHg/ml}$ $\tau_{\sigma,rv} = 1.5 \text{ s}$ $T_{e,rv} = 2 \text{ s}$ $G_{eff,rv} = 0.282 \text{ mmHg/ml/Hz}$
	Veins		$\tau_{\sigma,V} = 10 \text{ s}$ $T_{e,V} = 5 \text{ s}$ $G_{eff,V} = -275 \text{ ml/Hz}$ $V_0 = 3200 \text{ ml}$
	Arterioles		$\tau_{\sigma,R} = 1.5 \text{ s}$ $T_{e,R} = 3 \text{ s}$ $G_{eff,R} = 0.2 \text{ mmHg/(ml/s)/Hz}$ $R_0 = 0.3 \text{ mmHg/(ml/s)}$

Table A3 – Respiratory and chemoreceptor parameters

Variables	Value	Variables	Value
Lung		Brain	
Residual volume	1.2 L	Brain blood flow conductance	5.7 (L/min)/bar
Total lung capacity	6 L	Brain oxygen consumption rate	0.05 L/min
Functional residual capacity	2.4 L	Brain respiratory quotient	0.8
Effective moving mass of lung	0.5 kg	Total brain blood capillary volume	0.9 L
Lung constant effective surface area	0.125 m ²	Cardiac output time constant	6 seconds
Lung minimum effective surface area	0.105 m ²	Brain blood flow time constant	6 seconds
Lung elastance when lung at un-stretched region	5 cm water/L	Ratio between brain blood flow and cardiac output	0.15
Lung volume when lung stretched	5.5 L	Inspiratory time chemical controller gain	0.062
Maximum lung elastance	10 cm water/L	Expiratory time chemical controller gain	0.4
Viscous friction coefficient	500 N/(m/s)	Thoracic force integral gain for inspiration	335
Polytropic index	1	Thoracic force proportional gain for inspiration	6.7
Intra-pulmonary airway resistance	0.001cm water/(L/s)	Thoracic force integral gain for expiration	335
Fractional flow rate from right to left shunt	0.02	Thoracic force proportional gain for expiration	50
Solubility coefficient of N ₂ in blood	0.013 L/(L blood atm)	Time constant factor of demand lung profile	0.15
Solubility coefficient of He in blood	0.003 L/(L blood atm)	Thoracic force derivative term gain	10 ⁵
Saturated oxygen capacity in blood	0.2 L/L blood	Minimum thoracic force	-700N
Saturated carbon dioxide capacity in blood	1 L/L blood	Maximum thoracic force	700N
Nose		Mouth	
Equivalent diameter of nostril	22.5 mm	Effective diameter of mouth	22.5 mm
Width of linear flow region	0.0001 bar	Width of linear flow region	10 ⁻⁴ bar

Table A3 – Respiratory and chemoreceptor parameters (contd...)

Variables	Value	Variables	Value
Trachea			
Nominal radius of airway without traction	0.0001 m	Number of tracheobronchial airway	16400
Addition airway radius with airway traction	0.0002 m	Width of linear flow region	0.0001 bar
Trachea wall stiffness	7000 N/m	Closing lung volume	0.9 L
Length of moving tracheobronchial wall	0.001 m	Total lung capacity	6 L
Minimum radius of extra-pulmonary airway	0 m	Nominal radius of airway without traction	0.0001 m
Maximum radius of extra-pulmonary airway	0.0003686 m	Addition airway radius with airway traction	0.0002 m
Total volume of intra-thoracic zone	0.052 L	Trachea wall stiffness	7000 N/m
Total volume of extra-thoracic zone	0.123 L	Length of moving tracheobronchial wall	0.001 m
		Minimum radius of extra-pulmonary airway	0 m
Peripheral chemoreceptor		Central chemoreceptor	
Peripheral chemoreceptor constant k_1	-13.8	Central chemoreceptor constant k_4	1
Peripheral chemoreceptor constant k_2	0.182	Central chemoreceptor constant k_5	-18.118
Peripheral chemoreceptor constant k_3	828		

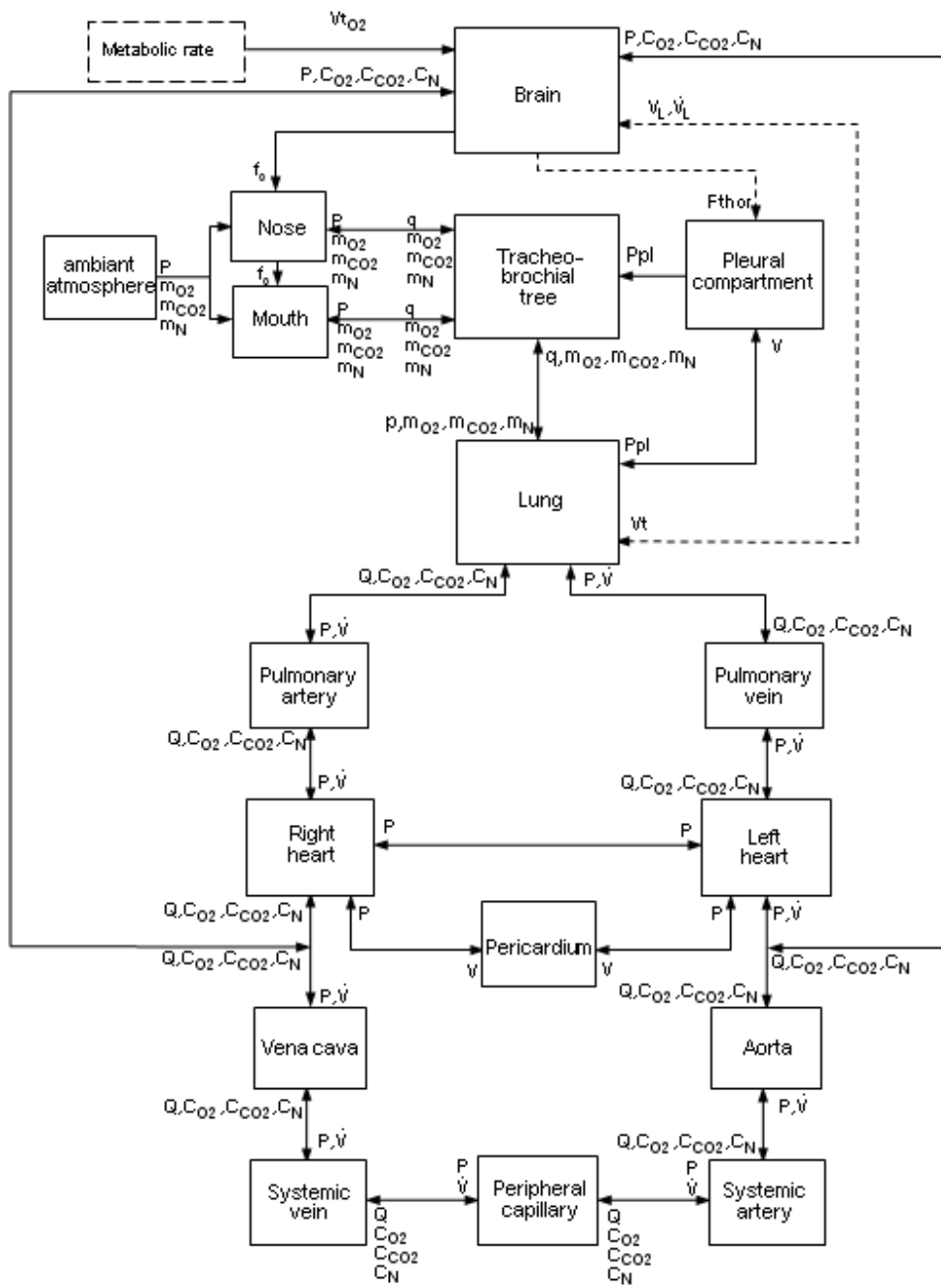


Fig. 1 Block diagram of the human cardiopulmonary system

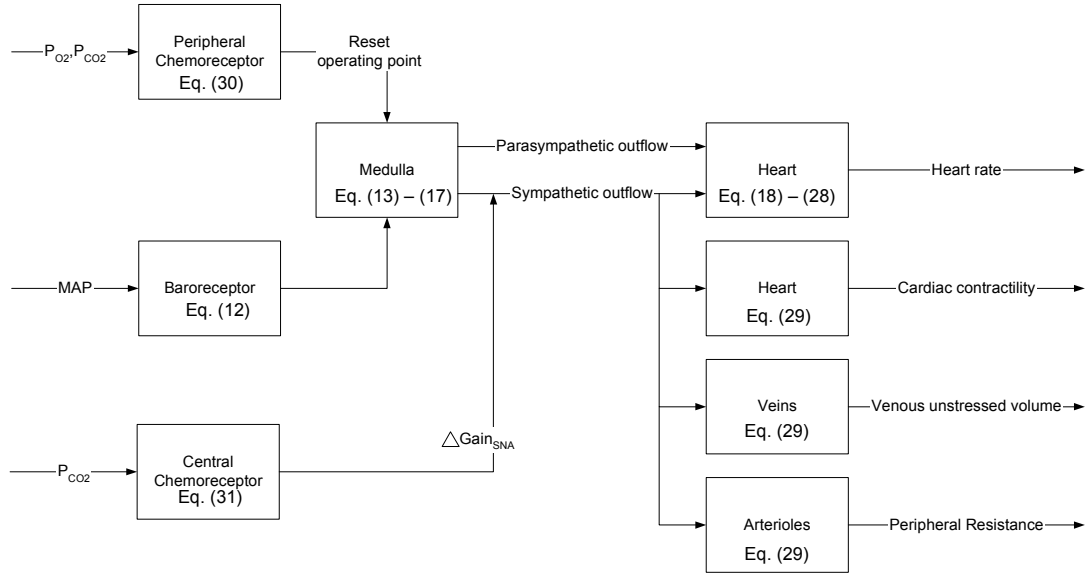


Fig. 2 Block diagram of the human baroreflex and chemoreflex control system
(Eq. refers to associated equations numbers in the text)

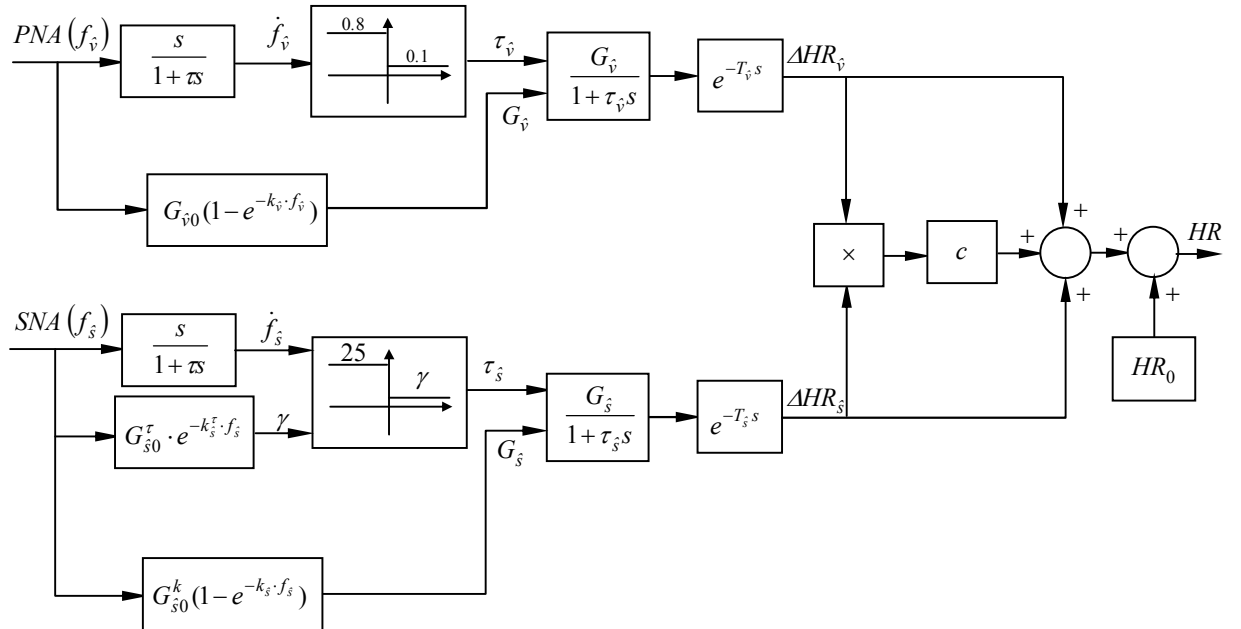


Fig. 3 Block diagram of heart rate control scheme (associated with Eqs (18) – (28))

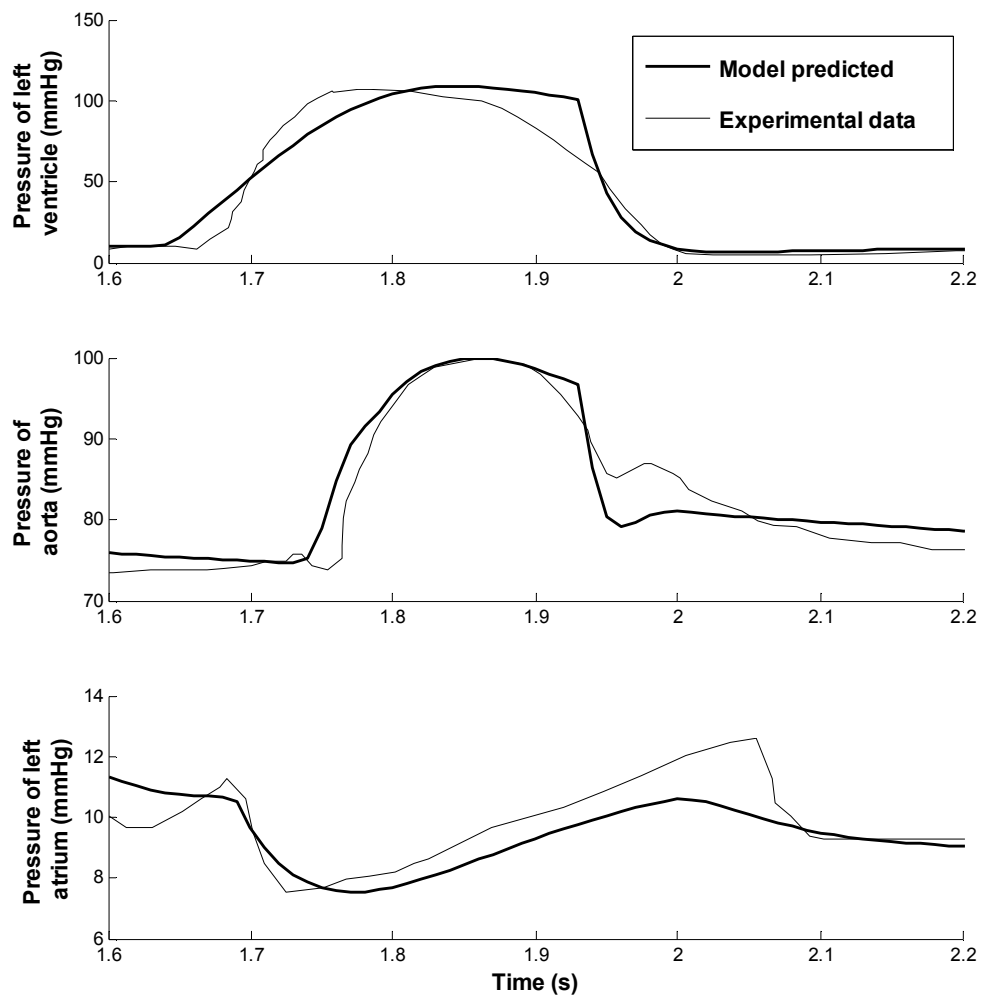


Fig. 4 Pressure of left ventricle, aorta and left atrium (Simulation results and experimental data taken Sugawara et al [33])

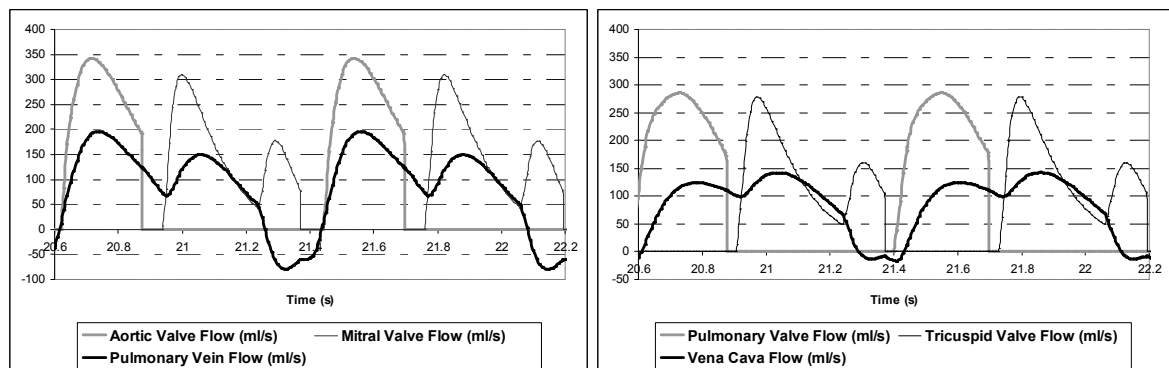


Fig. 5 Heart valve flow and venous return for left and right heart

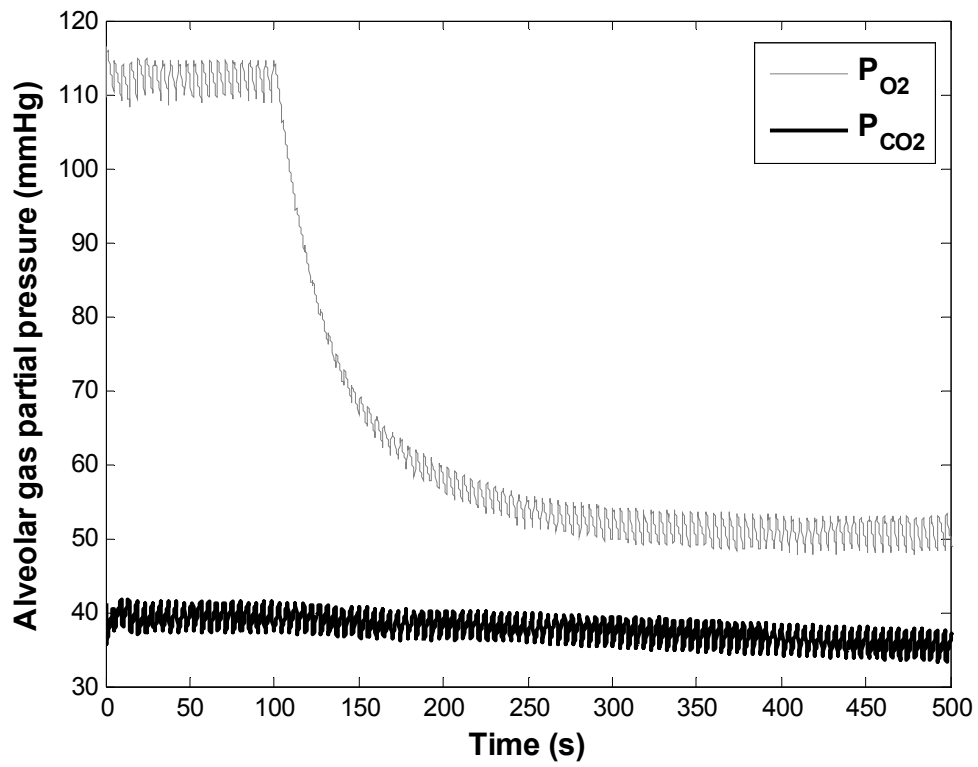


Fig. 6 Alveolar P_{O_2} and P_{CO_2} responses to hypoxia

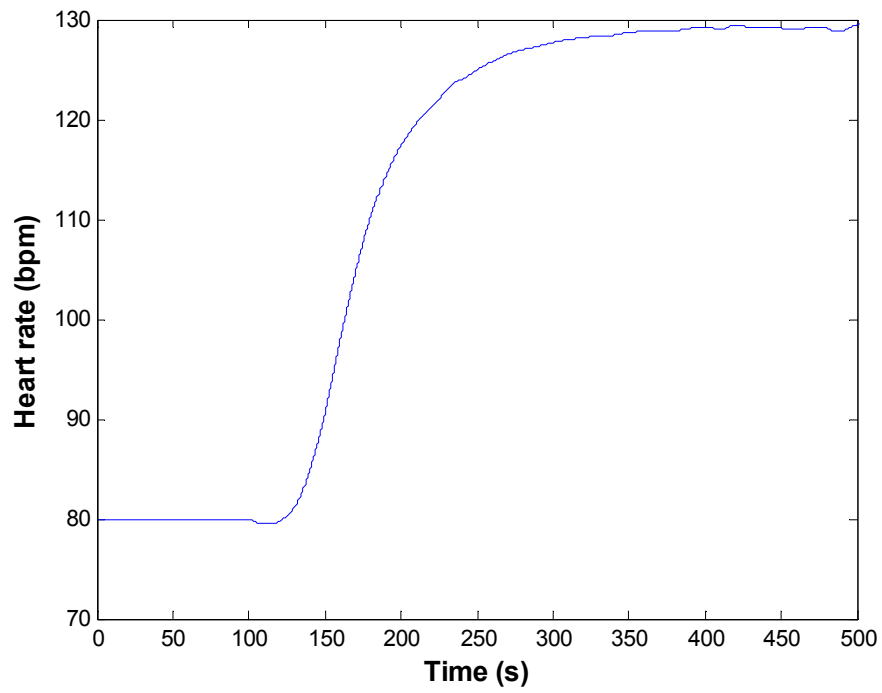


Fig. 7 Heart rate response to hypoxia with baroreceptor denervated

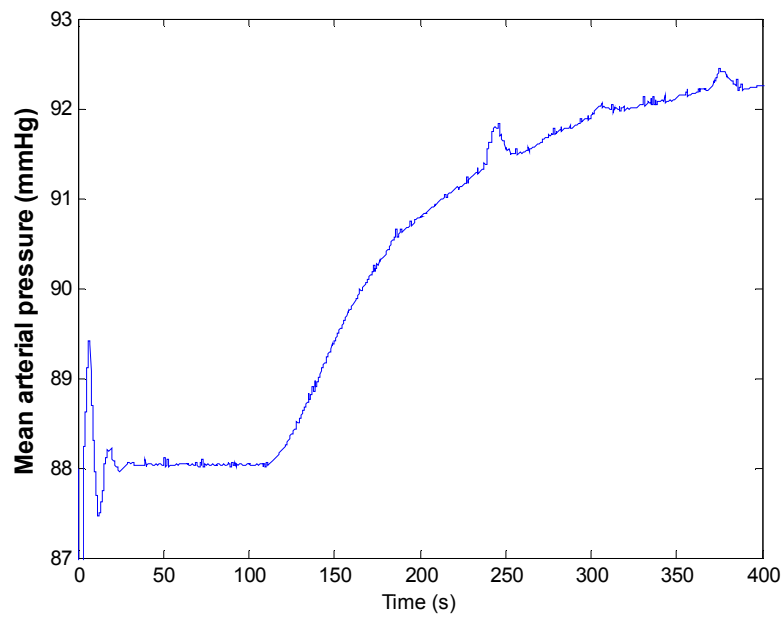


Fig. 8 Mean arterial pressure response to hypoxia with baroreceptor and chemoreceptor stimulated

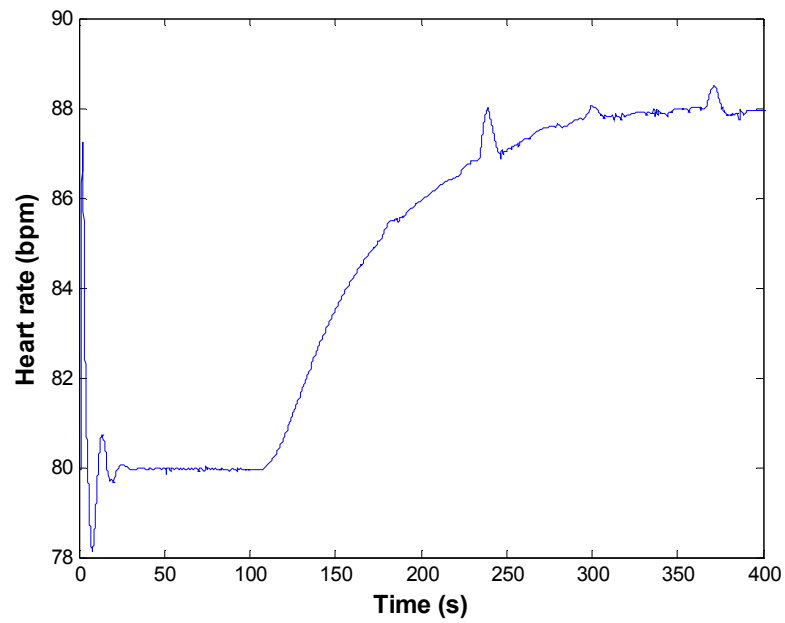


Fig. 9 Heart rate response to hypoxia with baroreceptor and chemoreceptor stimulated

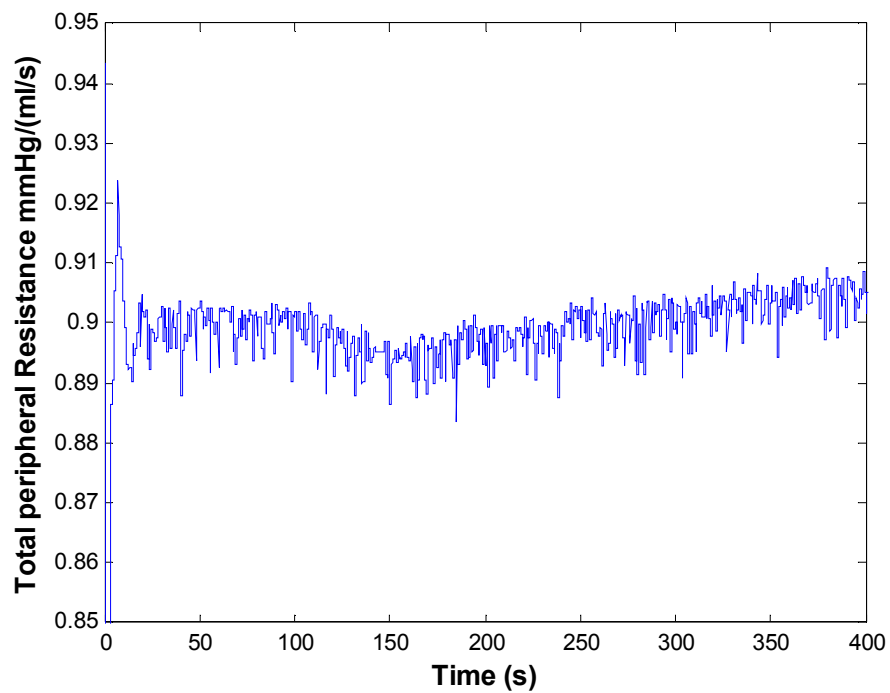


Fig. 10 Total peripheral resistance response to hypoxia with baroreceptor and chemoreceptor stimulated

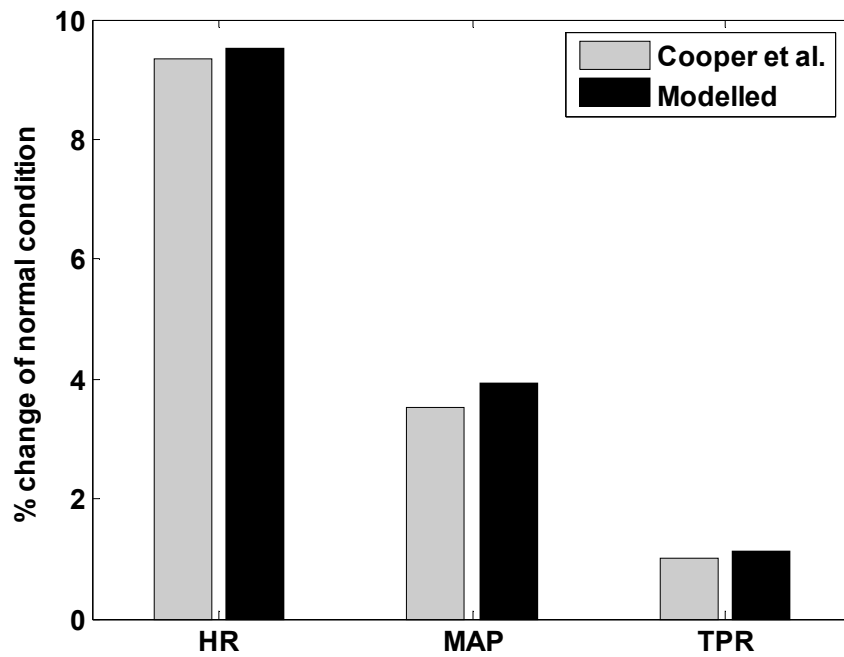


Fig. 11 Normalized values of heart rate (HR), mean arterial pressure (MAP), and total peripheral resistance (TPR) compared with experimental data from Cooper et al [35] during hypoxia

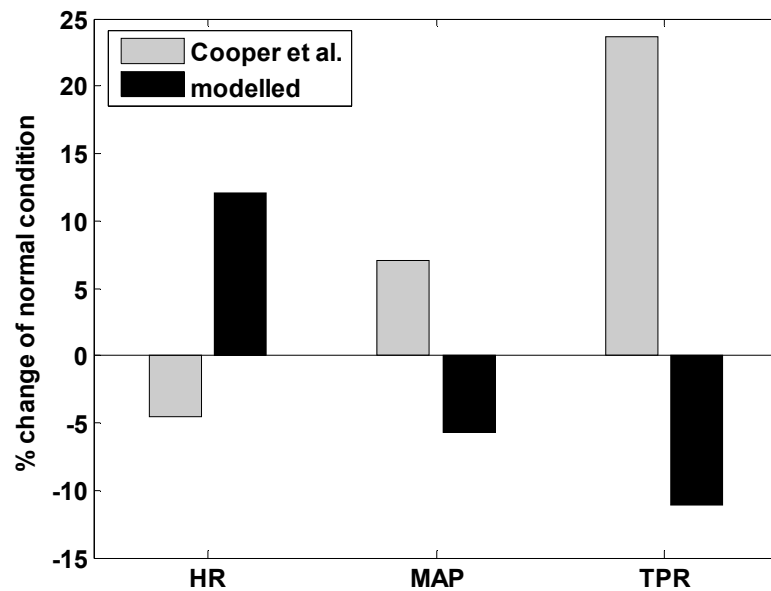


Fig. 12 Model predicted heart rate (HR), mean arterial pressure (MAP), and total peripheral resistance (TPR) compared with experimental data from Cooper et al [35] with denervated central chemoreceptor during hypercapnia

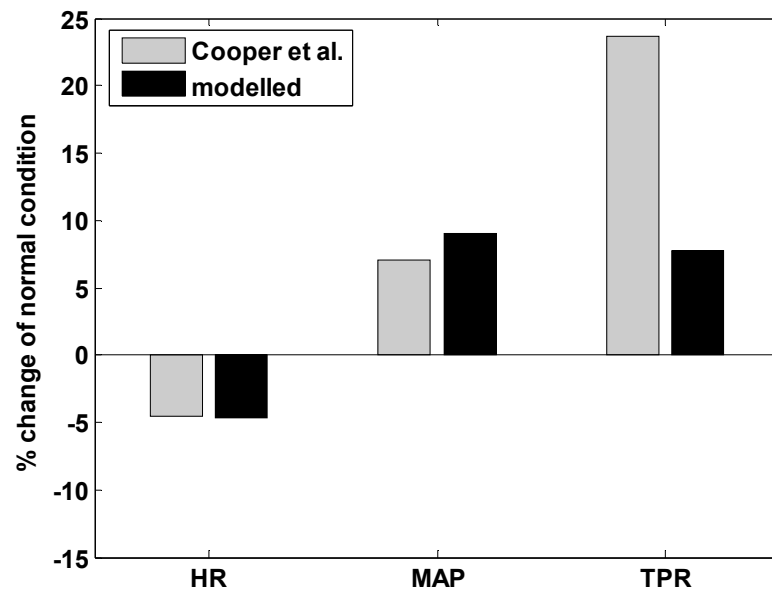


Fig. 13 Model predicted heart rate (HR), mean arterial pressure (MAP), and total peripheral resistance (TPR) compared with experimental data from Cooper et al [35] after innervated central chemoreceptor during hypercapnia

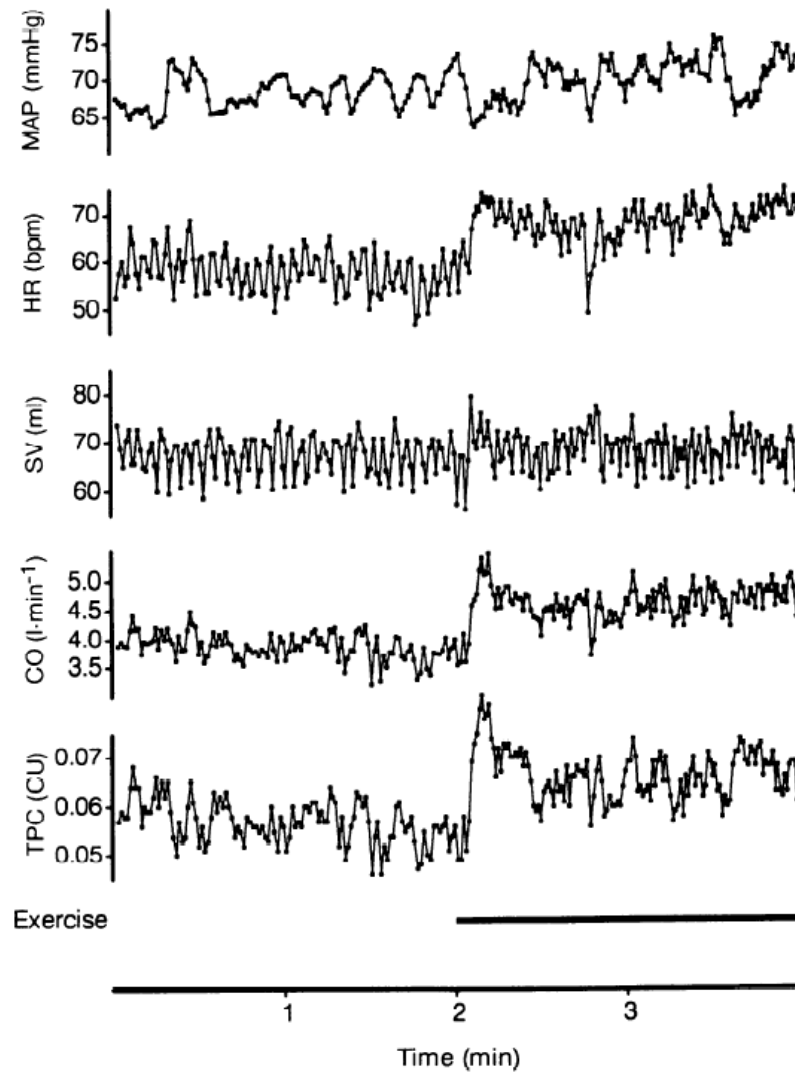


Fig. 14 Primary recording of cardiovascular variables from 1 typical experiment.
 MAP: Mean Arterial Pressure; HR: Heart Rate (beats/min); SV: Stroke Volume; CO: Cardiac Output;
 TPC: Total Peripheral Conductance (calculated by dividing CO by MAP, unit: $\text{l} \cdot \text{min}^{-1} \cdot \text{mmHg}^{-1}$) (Toska and Eriksen [36])

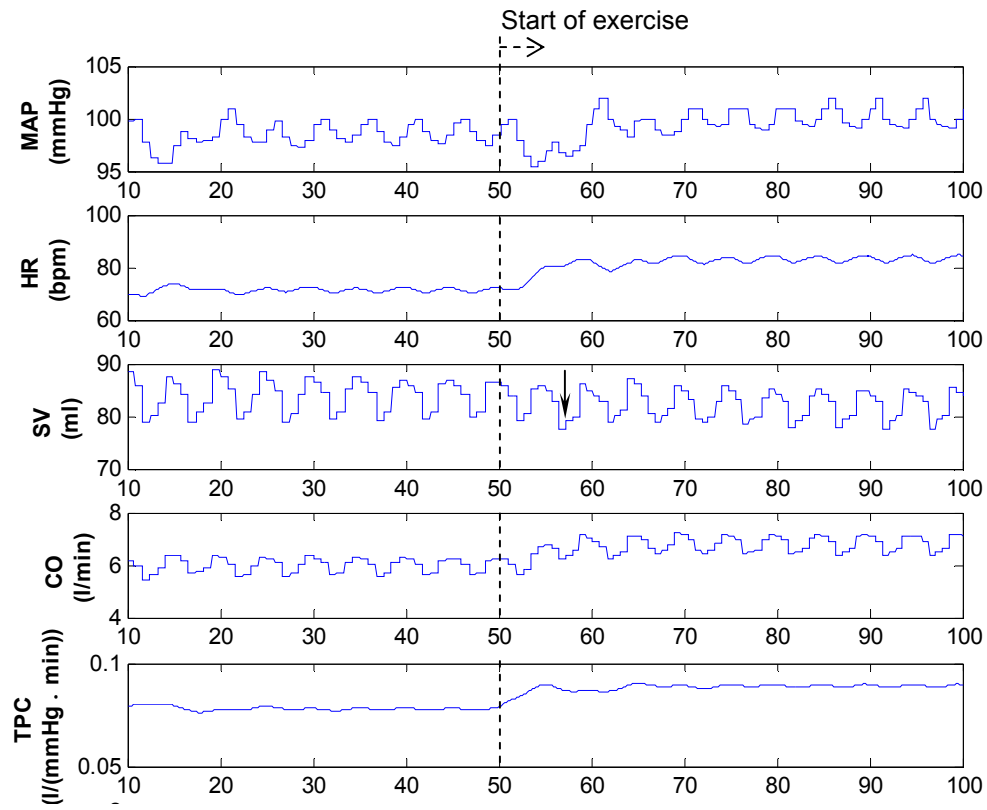


Fig. 15 Cardiovascular response predicted by the model.
MAP: Mean Arterial Pressure; HR: Heart Rate (beats/min); SV: Stroke Volume; CO: Cardiac Output;
TPC: Total Peripheral Conductance